NEBRASKA
Good Life. Great Journey.
DEPARTMENT OF TRANSPORTATION

Report FY21(012)

Field Demonstration of GPR and UAV Technologies for Evaluation of Two US 75/77 Bridges

Sepehr Pashoutani, Jinying Zhu, Chungwook Sim, Brendan Barnes

Department of Civil Engineering, University of Nebraska-Lincoln

July 2021

TECHNICAL REPORT DOCUMENTATION PAGE

1. Report No. FY21(012)	2. Government Accession No.	3. Recipient's Catalog No.
4. Title and Subtitle Field Demonstration of GPR and UAV Technologies for Evaluation of Two US 75/77 Bridges		**5. Report Date** May 2021 **6. Performing Organization Code**
7. Author(s) Sepehr Pashoutani, Jinying Zhu, Chungwook Sim, Ji Young Lee		**8. Performing Organization Report No.**
9. Performing Organization Name and Address Department of Civil and Environmental Engineering. University of Nebraska-Lincoln 1110 S 67th St., Omaha, NE 68182		**10. Work Unit No.** **11. Contract** FY21(012)
12. Sponsoring Agency Name and Address Nebraska Department of Transportation Research Section 1400 Hwy 2 Lincoln, NE 68502		**13. Type of Report and Period Covered** Final Report July 2020 – May 2021 **14. Sponsoring Agency Code**
15. Supplementary Notes		

16. Abstract

Two Nebraska bridges with asphalt overlay were selected for nondestructive testing and evaluation (NDT/NDE). Three NDT techniques were conducted on these two bridges, including Ground Penetrating Radar (GPR), Half-Cell Potential (HCP) and Unmanned Aerial Vehicle (UAV) imaging. NDT data were collected during three construction stages of the bridges: (1) before repair on existing asphalt overlay; (2) on bare concrete after asphalt removal; (3) and after repairing delaminated concrete.

A machine learning technique, autoencoder, was used to build quantitative relationships between different NDT datasets. On bare concrete, the GPR amplitude and HCP voltage show a strong linear relationship. Then a threshold for GPR amplitude (-6.4 dB) can be determined based on the well-established HCP criteria. The GPR amplitudes on asphalt overlay also show a clear correlation with GPR amplitudes on bare concrete. Direct comparison of two GPR amplitude maps indicates GPR data collected on asphalt overlay could detect most severely deteriorated areas but may miss some mild deterioration.

A big data image pipeline was created for mapping cracks and repair patches with images collected from an UAV. Comparing surface defects on asphalt overlay with HCP and GPR data suggests that UAV images may be used as an initial screening tool for extending NDT inspection of bridge decks. Further studies are needed to evaluate the performance of UAV imaging based visual inspection through quantitative analysis of surface defects and severity of deterioration.

17. Key Words	18. Distribution Statement
Nondestructive Evaluation (NDE), UAV, GPR, HCP, Machine Learning, Data Fusion	No restrictions. This document is available through the National Technical Information Service. 5285 Port Royal Road Springfield, VA 22161

19. Security Classification (of this report)	20. Security Classification (of this page)	21. No. of Pages	22. Price
Unclassified	Unclassified	38	

Form DOT F 1700.7 (8-72)	Reproduction of completed page authorized

DISCLAIMER

The contents of this report reflect the views of the authors, who are responsible for the facts and the accuracy of the information presented herein. The contents do not necessarily reflect the official views or policies neither of the Nebraska Department of Transportations nor the University of Nebraska-Lincoln. This report does not constitute a standard, specification, or regulation. Trade or manufacturers' names, which may appear in this report, are cited only because they are considered essential to the objectives of the report.

The United States (U.S.) government and the State of Nebraska do not endorse products or manufacturers. This material is based upon work supported by the Federal Highway Administration under FY21(012). Any opinions, findings and conclusions or recommendations expressed in this publication are those of the author(s) and do not necessarily reflect the views of the Federal Highway Administration."

Abstract

Two Nebraska bridges with asphalt overlay were selected for nondestructive testing and evaluation (NDT/NDE). Three NDT techniques were conducted on these two bridges, including Ground Penetrating Radar (GPR), Half-Cell Potential (HCP) and Unmanned Aerial Vehicle (UAV) imaging. NDT data were collected during three construction stages of the bridges: (1) before repair on existing asphalt overlay; (2) on bare concrete after asphalt removal; (3) and after repairing delaminated concrete.

A machine learning technique, autoencoder, is used to build the quantitative relationship between different NDT data sets. On bare concrete, the GPR amplitude and HCP voltage show a strong linear relationship. Then a threshold for GPR amplitude (-6.4 dB) can be determined based on the well-established HCP criteria. The GPR amplitudes on asphalt overlay also show a clear correlation with GPR amplitudes on bare concrete. Direct comparison of these two GPR amplitude maps indicates GPR data collected on asphalt overlay could detect all severely deteriorated areas but may miss some mild deterioration.

A big data image pipeline was created for mapping cracks and repair patches with images collected from an UAV. Comparing surface defects on asphalt overlay with HCP and GPR data suggests that UAV images may be used as an initial decision criterion for deploying and extending NDT inspection of bridge decks. Further studies are needed to evaluate the performance of UAV imaging based visual inspection through quantitative analysis of surface defects and severity of deterioration.

Acknowledgments

This research project has been sponsored by the Nebraska Department of Transportation. The authors would also like to acknowledge the engineers at the Department of Transportation for their assistance in this project, and specifically Kent Miller, Mark Traynowicz, Fouad Jaber, Jeff Francis, and Jason Volz, for providing the bridge information and the arrangements of traffic controls in the field testing. In addition, the authors would like to thank Vector Corrosion Services, Inc. engineers for collecting and providing the half-cell potential data.

Contents

List of Figures

List of Tables

Chapter 1

Introduction

1.1 Background

Asphalt overlay on top of a waterproofing membrane (ACC&M) is increasingly applied on many bridges in the United States. ACC&M offers an extra layer of protection to concrete deck and increases the service life of structure by reducing the traffic-induced stress on concrete and concrete exposure to chemicals. However, asphalt overlay hinders visual inspection of the concrete deck surface and limits applications of many nondestructive testing (NDT) methods. If a breach of the waterproofing membrane occurs, ingression of chloride agents into concrete over time may initiate corrosion of steel reinforcement. Many State DOTs perform visual inspection of the wearing surfaces to identify the deterioration of overlays. The types of defects may include debonding, delamination, spalls, patches, potholes, cracks, abrasion, wearing, rutting, distortion, or section loss, etc. In a previous research project (M075), the authors showed that there is a strong correlation between visible transverse cracks on concrete surface and deteriorated areas detected by ground penetrating RADAR (GPR) and Vertical Electrical Impedance system [1]. For bridge decks with asphalt overlay, it is important to understand how surface defects on the asphalt overlay are associated with internal condition of the concrete. Therefore, we need to collect NDT data on decks with and without the asphalt overlay and to determine the relationship between them.

Uncertainties in NDT data and defects identification depend on the NDT technique, types of defects, and environmental factors during the field testing. Using multiple NDT technologies may increase reliability of concrete defect assessment and severity of deterioration [1–3].

According to the American Society for Testing and Materials (ASTM) D6087 standard [4], GPR is currently the only proven NDT method to evaluate a concrete bridge deck with asphalt overlays. GPR has been widely used for condition assessment of bridge decks by measuring rebar reflection amplitude and variation of electrical permittivity and conductivity of concrete over the bridge deck [5, 6]. This unique feature in GPR helps identify areas on the bridge deck that are susceptible to reinforcement corrosion without removing asphalt layer. Ground-coupled GPR antenna provide high quality data and reliable assessment of bridge decks. However, ground-coupled GPR data collection can only be conducted at a walking speed and requires traffic control for bridge evaluation.

Half-Cell Potential (HCP) is the standard test method for measuring the probability of corrosion in reinforced concrete structures. HCP measures the electric potential between top reinforcement mat and a probe on concrete surface. Since GPR and HCP work based on electrical properties of concrete, they are expected to provide similar results when used on the same bridge deck. However, no quantitative comparison can be found in literature between GPR amplitudes collected on asphalt overlay and HCP on the bare concrete after removing the asphalt. Providing this comparison should help transportation agencies and consulting companies to better interpret GPR data based on well-established HCP technique.

From a survey conducted by the American Association of State Highway and Transportation Officials (ASSHTO) in 2019, it was found that 36 state Department of Transportation (DOT) had researched and/or used UAVs for their bridge inspections, surveying, and monitoring and mitigating risks posed by landslides or flooding [7], which increased from 17 states in 2018. Nebraska DOT has started investigating the feasibility of UAV implementation in inspection procedures and started developing drone polices. In studies that investigated the viability of UAV for bridge inspection in Michigan and Minnesota, both states indicated that the benefits would include improving safety of the manual inspection procedure which typically involves bringing heavy equipment, detouring traffic, and setting up work zones while UAVs can get in and out quickly without obstructions. The benefits increase when UAVs can access areas that it is difficult to inspect (underneath the bridge or to a high truss member, etc.) for human inspection.

In addition, there has been constant effort in applying machine/deep learning models to detect damages for the past decade [8–15] with images of structural members. Most of the previous research focused on testing out crack detection algorithms and the limitation exists because the models were implemented only for a local region. In this project, a deep learning model was implemented for the image data analysis using image data collected from UAVs and the difference with previous research is that the research team at UNL

focused on developing a model that can be applied to a larger scale for the entire structural member which is rarely demonstrated in other research studies.

1.2 Objectives and Research Task

GPR is an effective NDT method to evaluate deterioration of bare concrete bridge decks. GPR can also be used on asphalt overlaid bridge decks. However, the test efficacy and reliability need further investigation because the overlay brings additional uncertainties to the data interpretation. In addition, asphalt overlay hinders direct visual inspection of concrete surface and application of many other NDT methods.

In this study, the research team applied three NDT methods, GPR, HCP, and UAV imaging to two Nebraska bridges. GPR and UAV imaging data were collected before and after bridge deck repair on both asphalt overlay and bare concrete decks, and HCP data were collected on the bare concrete after asphalt removal. The HCP test was used as the ground-truth in this research to evaluate the performance of GPR test. Research objectives and main tasks are shown below.

- Although GPR is an effective NDT technique on bare concrete bridge decks, determination of threshold amplitude is still a challenging topic to distinguish deteriorated areas from sound in reinforced concrete. In this study, the GPR data were correlated to the HCP data to determine the threshold amplitudes.
- The asphalt layer causes additional attenuation of GPR signals and alters the threshold amplitudes that were obtained from GPR survey on bare concrete decks. In this project, GPR data collected on asphalt overlaid decks were compared to the HCP and GPR data on bare concrete, in order to determine the threshold amplitudes for GPR on asphalt.
- For quantitative comparison of NDT data (GPR and HCP) and obtaining threshold amplitudes, many assumptions regarding the type of relationship are needed. To prevent bias and increase generality, machine learning models were built to obtain quantitative relationships between different data sets.
- The asphalt layer hinders visual inspection of concrete deck surface. To investigate if defects on asphalt surface might be indicative of internal concrete deterioration, a UAV imaging system was flown over the bridge and captured localized image from the deck surface with and without the asphalt layer. Localized images were stitched together with a commercial software and a stitched image for the entire bridge deck was generated. Later, location of visible surface defects including spalls and potholes

were extracted and compared with the GPR and HCP data.

1.3 Report Overview

This report outlines the findings of the research conducted by University of Nebraska-Lincoln (UNL) research team with the support from Nebraska Department of Transportation (NDOT). **Chapter 1** summarizes the research objectives, and the background information of NDT technologies in condition assessment of bridge decks. **Chapter 2** presents the working principle of three NDT techniques, GPR, HCP and UAV imaging and their application to bridge deck evaluation. **Chapter 3** presents the result of the three NDT technologies deployed on two Nebraska bridges with asphalt overlay. Conclusions and implementation plan of this research project are presented in **Chapter 4** .

Chapter 2

Nondestructive Testing Techniques and Data Analysis

2.1 Ground Penetrating Radar

Ground Penetrating Radar is a widely accepted NDT technique to identify the steel corrosion and potential deterioration in concrete bridge decks. A GPR system generally consists of a control computer and an antenna. The computer provides power to the antenna, set measurement parameters, and stores recorded data. The antenna box contains a transmitter module to send electromagnetic pulse and a receiver to receive echoes from the surface and subsurface interfaces. Meanwhile an external Real-Time Kinematic (RTK) GPS system attached to the GPR survey cart provides real-time positions during the scanning.

A survey cart, shown in the **Figure 2.1**, was used in ground-coupled GPR survey. Since ground-coupled GPR survey can only be conducted at a walking speed, traffic control is needed. The center frequency of the antenna determines the maximum penetration depth of EM wave and the vertical resolution of the B-scan image. Increasing the frequency will improve the image resolution at the cost of decreasing the penetration depth. In most bridge deck surveys, ground-coupled antennas with a center frequency of 1.5 GHz provides sufficient penetration depth and adequate resolution. The time range determines the total time that GPR records for the reflections from the subsurface. The proper time range can be determined by the expected penetration depth and velocity information.

(a) GSSI SIR-4000 computer **(b)** GPR system on a survey cart

Fig. 2.1. GSSI-4000 GPR system.

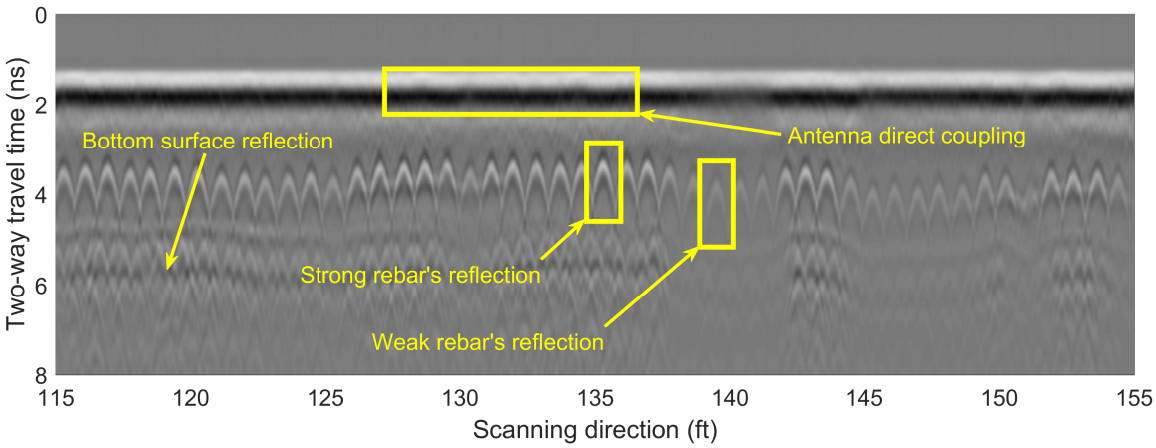

Fig. 2.2. GPR B-scan image

Figure 2.2 shows a GPR B-scan images recorded on a bridge deck with 8 ns time range in the vertical scale. As highlighted in **Figure 2.2**, direct coupling, rebar reflection, and bottom of the bridge deck are the main features that can be visually identified in the image. The conventional GPR analysis method is to analyze B-scans through comparison of depth-corrected amplitudes of rebar reflections. Concrete deterioration and rebar corrosion will decrease the GPR amplitude and increase attenuation. Therefore, GPR amplitude (or attenuation) map is most commonly used to represent deterioration of bridge deck.

The UNL research team recently proposed a complete procedure for GPR data processing to automate GPR data analysis. Major improvements include accurate zero offset, migration

of rebar reflections, amplitude correction based on actual rebar depth, and accurate wave velocity, etc. Details can be found in recently published research reports and publications [16, 17].

2.2 Half-Cell Potential

HCP testing is the standardized test method in ASTM C876 [18] for measuring the probability of corrosion of uncoated steel reinforcement in concrete structures. An electrode of the HCP device forms one half of the cell from concrete surface and the reinforcing steel rebar in the concrete form the other half cell. The behavior of steel in concrete can be characterized by measuring its half-cell potential. Figure 2.3 shows the working principle of HCP methodology. The chances of corrosion forming on the steel in concrete and half-cell potential are directly proportional, the higher the potential, the higher the risk of corrosion on steel reinforcement. Although the principles of HCP testing are rather simple, the procedure is time-consuming which requires drilling a hole in concrete to make a connection to the steel reinforcement.

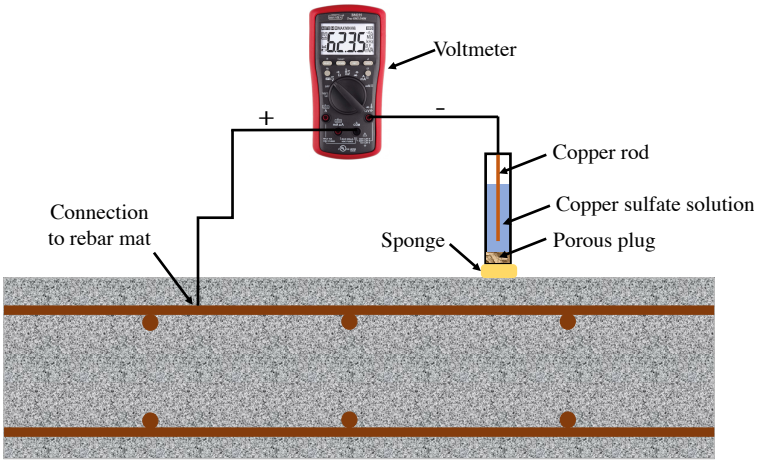

Fig. 2.3. Schematic working principle of HCP

2.3 Unmanned Aerial Vehicle Imaging Analysis

With the increase in UAV implementation for bridge inspection, a big data image pipeline for mapping cracks and patches of repair was constructed by the research team. The typical

three steps of the image-based data processing pipeline would include 1) Data Collection, 2) Data Analytics, and 3) Data Management processes. The data collection step includes image collection with a commercial UAV. In this project, DJI Mavic Pro quadcopter was used for the UAV and the DJI Ground Station Pro (DJI GS Pro) was used to efficiently create waypoint flight paths, and flight zones for the area of interest. Then as the next step, for localization, a commercial photogrammetry software, Pix4D was used to reconstruct the 3D points and create a stitched image map from the image dataset collected from the UAV. Up to this data collection procedure, commercial tools were used which can easily be adapted by any UAV pilot/engineer who has license from the Federal Aviation Administration (FAA).

The pipeline development from our research team has mainly focused on building the next steps of the pipeline with data analytics and data management processes. The research team used a region-based Mask R-CNN[19] deep learning algorithm for conducting instance level segmentation of a given image. Mask R-CNN is an extended version of the Faster R-CNN[20] which can extract features and Region-of-Interests (RoIs). Once the features and RoIs are identified within a given image, mask prediction, bounding box regression, and label classification can be performed simultaneously within the neural network. To make predictions (find deficiencies or target objects such as cracks, spalls, pot holes, or patches), training and validation takes place with the sliced images (512 by 320 pixel pieces), that are pre-processed (based on a threshold image where exposure of the image can be adjusted), and fed into the neural network.

The data management procedure involves creating a database for the deficiencies identified from the data analytics step. For example, if the target deficiency is a crack, this step will collect all mask end points that were found from the Mask R-CNN model and create a JavaScript Object Notation (JSON) formatted file, initially. Then, the data plotter will plot and fill each individual mask on a blank 512 by 320 image to create a binary fill (crack or non-crack). As a next step, the data analyzer will construct Euclidean Distance Transform (EDT) from each mask, and construct binary skeletons for each mask, index the EDT using non-zero points in the binary skeletons to obtain skeleton with pixel unit crack measurements along the center line of the crack, and finally construct a heat map showing the indexed (relative) crack measurement data. Finally, additional to the crack DB, for visual conformation, the crack mapper will take positions of masks and plot all target predictions (for example, cracks) on the original sliced image and these images are stitched back together to create a global crack map. Figure 2.4 shows the overall process of the UAV Image-based big data pipeline introduced in this section.

Fig. 2.4. Summary of the UAV image-based big data pipeline

2.4 Data Analysis

Transportation agencies are increasingly using multi-sensor data collections to evaluate the bridge structures for rehabilitation and bridge infrastructure management [1, 21]. Multi-sensor data provides complementary information about bridge deck conditions and may give more accurate evaluation than an individual method may provide. However, quantitative comparison and visualization of multi-sensor data are still challenging. For example, unlike controlled laboratory environment, many unpredictable factors can influence field testing data and make interpretations difficult. Data fusion, as a systematic way of incorporating multi-sensor data, can help increase the reliability of data and reduce uncertainties. In this project, an autoencoder-based data fusion technique is used to reduce the noise from pairs of multi-source data to obtain a clear relationship. For example, based on the relationship between GPR and HCP data, a threshold amplitude with regard to the threshold potential of HCP (-350 mV) can be determined.

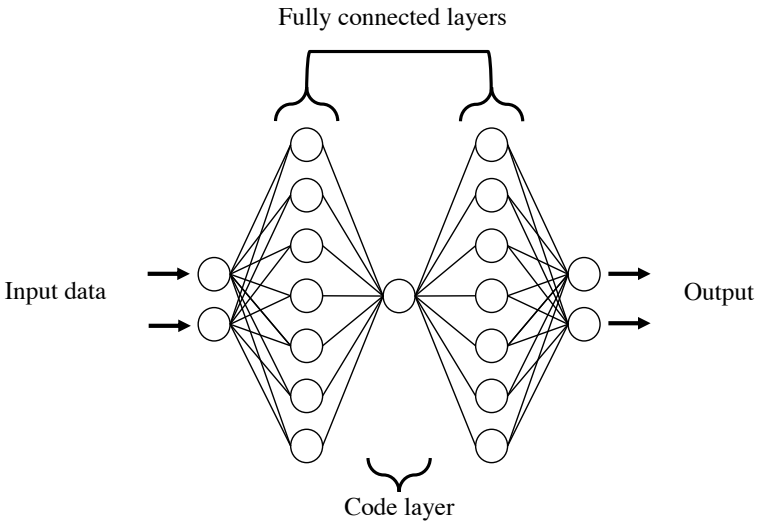

Fig. 2.5. Schematic diagram of autoencoder

2.4.1 Autoencoder

Autoencoders are classified among unsupervised Machine Learning (ML) models that are trained to copy input data. One of the major applications of autoencoder is nonlinear principal component analysis (NLPCA). Figure 2.5 shows the architecture of a simple autoencoder. Autoencoder consists of two main parts: Encoder and Decoder. The Encoder

transforms the input data into the Code layer, which has lower dimension than input data. The Decoder part reconstructs the original inputs from the Code layer. In complex problems, autoencoder can eliminate noise from the data and be used as a regression model.

2.4.2 Previous results from M075 project

In research project M075, sponsored by NDOT, the UNL team collaborated with a research team at Brigham Young University (BYU) to test three bridges using multiple NDE technologies [1, 22]. The three bridges have different types of overlays: no overlay, concrete overlay, and asphalt overlay. The UNL team collected GPR data and high-definition (HD) images using a vehicle-mounted imaging system. The BYU team performed vertical impedance (VEI) test. Since both GPR and VEI measure electrical properties of concrete, results from these two tests are expected to show high correlation.

Extensive data analyses were performed for bridge S077 05693R, which has a concrete overlay. To establish the relationship between GPR and VEI measurements, we selected GPR and VEI data collected from the same positions on Bridge S077 05693R for autoencoder training. Figure 2.6 shows the scattered plot of GPR and VEI data before (Input layer) and after (Output layer) autoencoder training. The output data shows much less scattering and gives a clear nonlinear relationship between the GPR and VEI data. This relationship was used to convert the remaining GPR data to VEI format, or vice versa. The converted GPR or VEI data can then be combined to form a fused NDE map. Compared to individual GPR and VEI maps, the fuse map has all critical features, but also shows additional features that were not observed on each individual map. Figure 2.7 shows the fused GPR and VEI map overlapped with identified surface cracks. The cracks detected by the HD imaging match the GPR/VEI detected deterioration areas very well. The research findings show that combining multiple NDT data sets can improve the accuracy and resolution of bridge deck evaluation.

In this project, we will use the similar autoencoder model to build the relationship between GPR and HCP data obtained on bare concrete deck, which can be used to determine proper threshold amplitudes for GPR data.

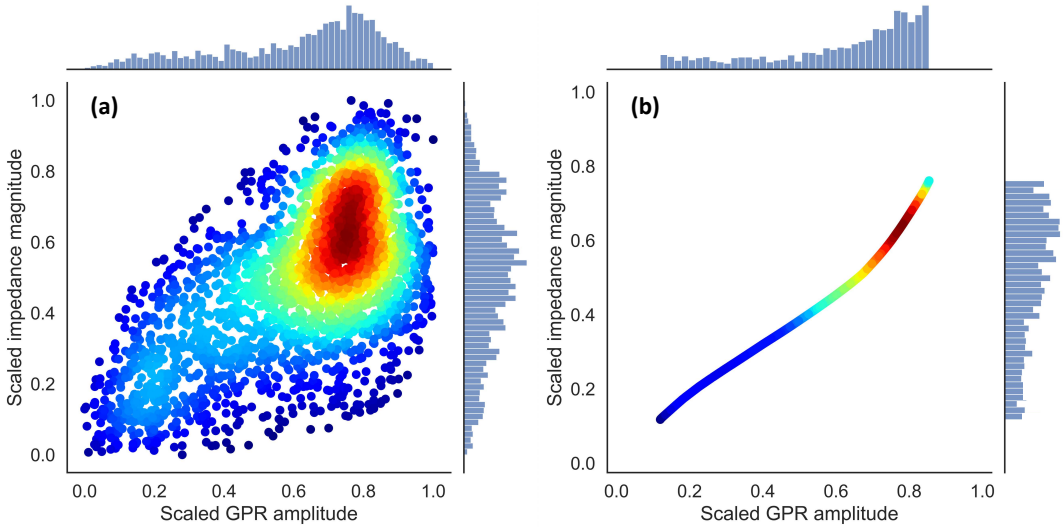

Fig. 2.6. Scatter plot of GPR vs. VEI data at the same locations on bridge S077 05693R: (a) scaled value of original input data and (b) autoencoder output

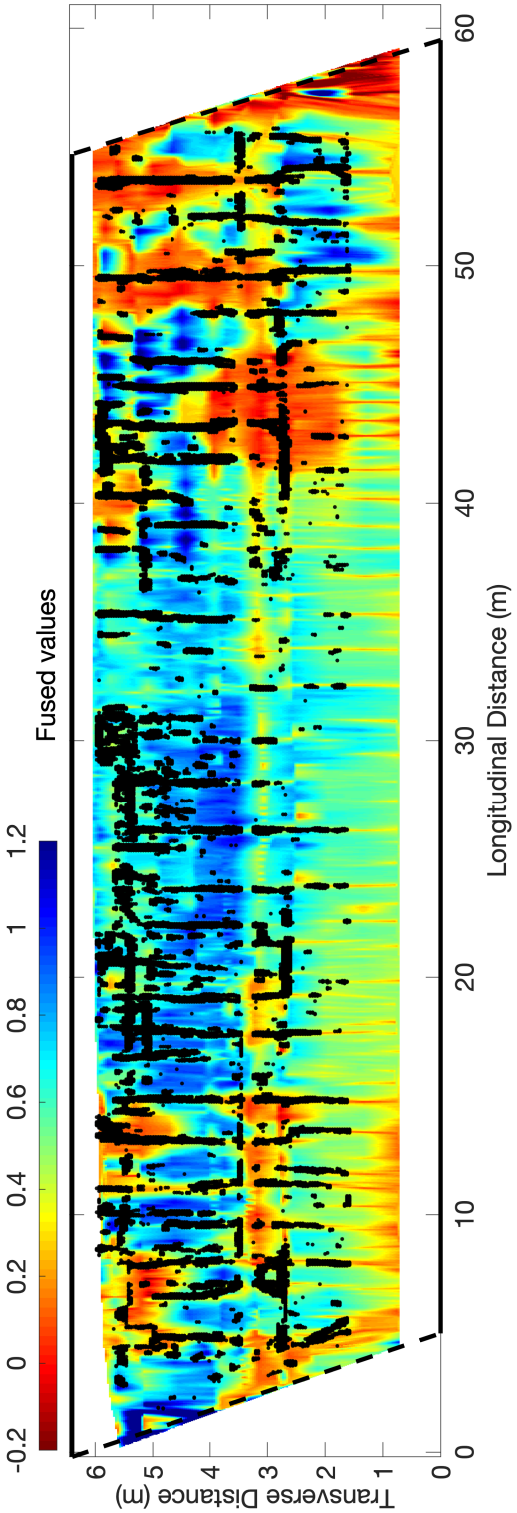

Fig. 2.7. Identified cracks overlapped on the fused GPR/VEI map (Bridge S077 05693R in M075 project)

Chapter 3

Field Demonstration

3.1 Bridge Information and Test Plan

Fig. 3.1. Location of two bridges for NDT evaluation

Two bridges were selected by NDOT for NDT data collection: S075 17596 and S075 17062. Both bridge decks were reconstructed in 1974 with asphalt overlay and waterproofing membrane. Figure 3.1 shows the locations of both bridges on the Google map. The bridge

information is shown in Table 3.1.

Table 3.1. Bridge information: S075 17596 and S075 17062.

Bridge ID	**S075 17596**	**S075 17062**
Total length	151.9 ft	60 ft
Width	40.0 ft	44.0 ft
Year built	1933	1938
Year reconstructed	1974	1974
Condition	Fair*	Fair*

Similar test plans were scheduled for both bridges. Data collection was performed in three stages of construction: (1) before removal of existing ACC&M overlay on August 24, (2) on bare concrete after removing the overlay on August 27, and (3) on bare concrete after repairing delaminated concrete and before placement of a new ACC&M overlay on September 18. On August 24, GPR and UAV data were collected on existing overlays. On August 27, the UNL team collected GPR data on bare concrete decks after asphalt was removed. On the same day, a team of engineers from Vector Corrosion Service Inc. collected HCP data from two bridge decks. On September 18, the UNL team collected GPR data and UAV images from both bridges on concrete surface after the decks were repaired with concrete patches. Table 3.2 shows the summary of NDT tests at three construction stages on both bridges.

Table 3.2. Summary of field data collection

NDT	Bridge S075 17596			Bridge S075 17062		
	08/24	08/27	09/18	08/24	08/27	09/18
GPR	✓	✓	✓	✓	✓	✓
UAV	✓		✓	✓		✓
HCP		✓			✓	

3.2 Bridge 1: S075 17596

3.2.1 Information

Bridge S075 17596 is located on US75/US77 over Omaha Creek in Nebraska, United States. Figure 3.2 shows the satellite image of the bridge. The bridge has three spans, with

a length of 151.9 ft and a width of 40 ft, and carries two-way traffic. The rebar spacing in transverse direction is 10 in for most locations. In 1974, the bridge was reconstructed and two shoulders were added to existing lanes. After widening, the bridge received asphalt overlay on a waterproofing membrane. In 2010, a paving project partially removed and replaced the ACC&M overlay. This work was not completed to meet the current or previous standard.

In Figure 3.2, the red lines highlight the GPR scan region on asphalt overlaid deck on August 24. The blue dashed lines indicate the boundaries of GPR scan region on August 27 and September 18. In all GPR scans, the spatial resolution was set as 3 mm in the longitudinal direction and line spacing of 1 ft in the transverse direction. HCP data was collected on concrete surface after asphalt removal on August 27. UAV images were collected on asphalt surface before repair and on concrete surface after repair. Refer to Table 3.2 for details.

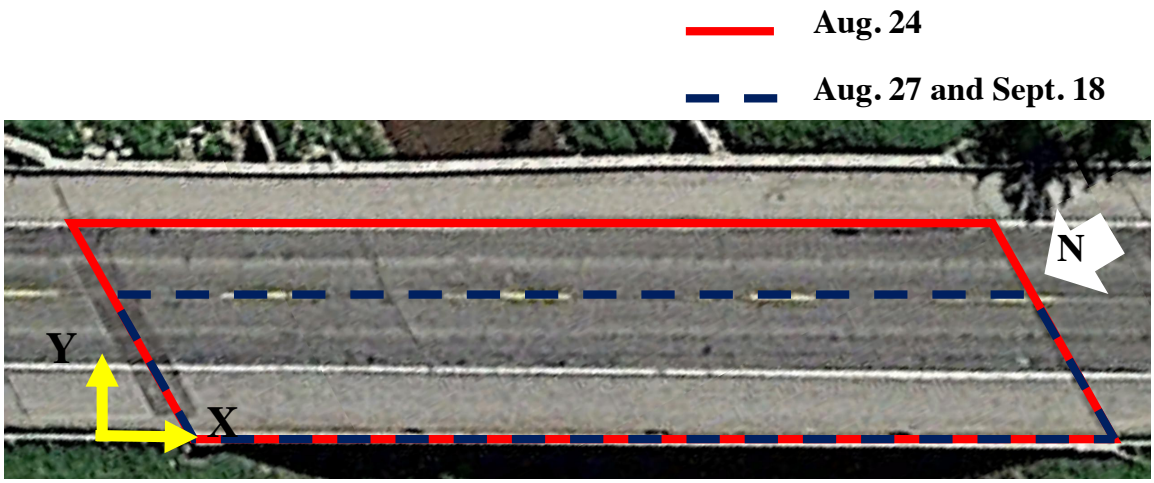

Fig. 3.2. Satellite image of bridge S075 17596

3.2.2 NDT results

Ground Penetrating Radar

Figure 3.3a shows the GPR amplitude map based on data collected on bridge S07517596 deck with existing asphalt overlay. The black lines show the boundaries of western lane and shoulder. In this map, low amplitude areas are shown with red color to indicate deck deterioration. Low amplitude is also observed along a horizontal line at 10 ft in transverse

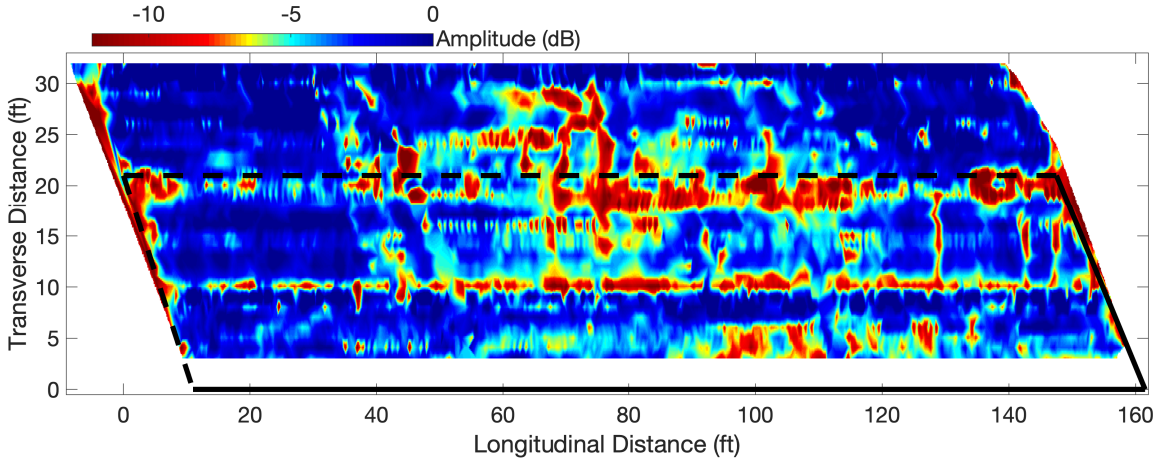

(a) On asphalt overlay

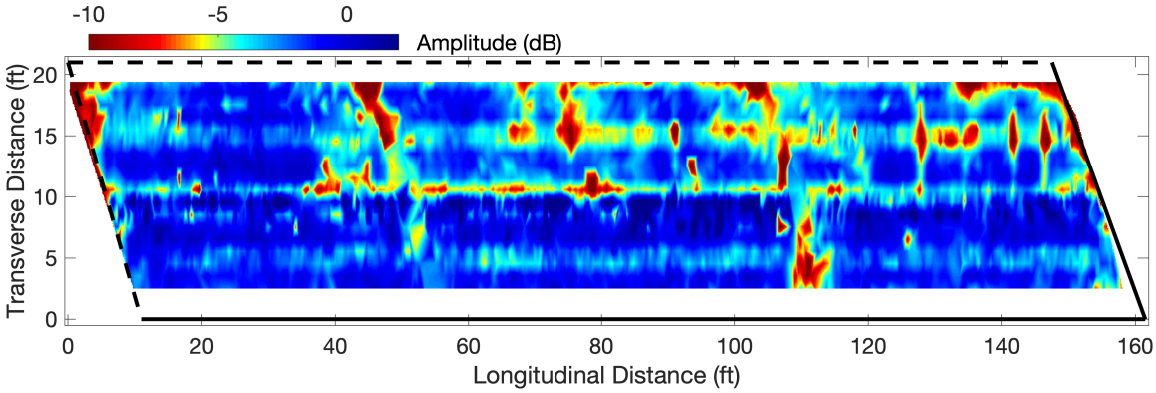

(b) On concrete before repair

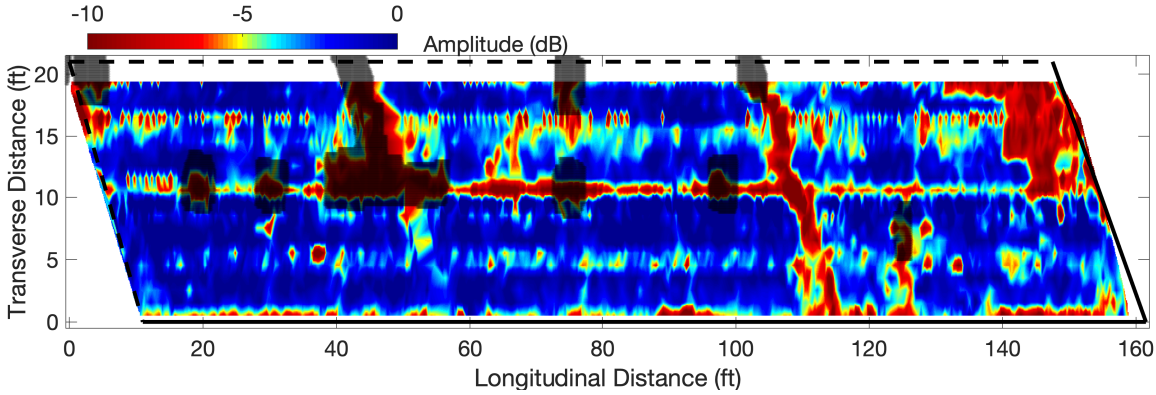

(c) On repaired concrete

Fig. 3.3. GPR amplitude maps from bridge S075 17596 in three construction stages

direction, which corresponds to the construction joint between the shoulder and driving lane. Major low amplitude regions in driving lane extends from 40 ft to 120 ft in longitudinal direction and along two end joints.

Figure 3.3b shows the GPR amplitude map using data collected on the western lane and shoulder of the bare concrete deck after the asphalt overlay was removed. Similar to the map with the asphalt overlay, low amplitudes occurs along the shoulder joint at 10 ft in transverse direction. Deterioration is also observed along two more horizontal lines at 5 ft and 15 ft in transverse direction, which are also observed on the map of asphalt overlaid deck but with less clarity. Although the map on bare concrete gives less severe deterioration than the map on asphalt overlay, both maps highlight the same deterioration regions.

Figure 3.3c shows the GPR amplitude map of the bridge deck after repairing delaminated regions detected by chain drag test. Figures 3.3b and 3.3c are very similar, except for the repaired regions marked by the transparent dark color. Since the new concrete patches were still wet during the GPR testing, they are shown as red color due to high attenuation of GPR signals in wet concrete. These patches should not be misinterpreted as defects.

Half-cell potential

HCP data was collected on a grid of 2 by 2 ft on the bridge deck after the asphalt layer were removed. In order to make the electrical circuit, a hole was drilled through the concrete cover to the top rebar level. Figure 3.4 shows HCP potential map of the bridge deck obtained from the western lane and shoulder as indicated by the dashed lines in Figure 3.2. The HCP map indicates a major portion of the driving lane has higher probability of corrosion activity than the shoulder. Similar to GPR maps, shown in Figures 3.3a and 3.3b, most highly negative potential regions are observed from 40 ft to 120 ft in longitudinal direction and along the horizontal line at 15 ft.

Unmanned Aerial Vehicle Imaging Analysis

A total number of 353 images were collected on August 24 from the first bridge (S075 17596) for a 40 minute data collection time, and 231 images were collected on September 18 from the same bridge for a 30 minute data collection time. Approximately 10,900 square feet of area was covered from each data collection. In the first data collection conducted on the asphalt overlay bridge on 8/24, although more images were collected, only 70% of the images had sufficient features to allow stitching for the calibrated images. The data collected on this day with the UAV had some limitations because traffic was controlled

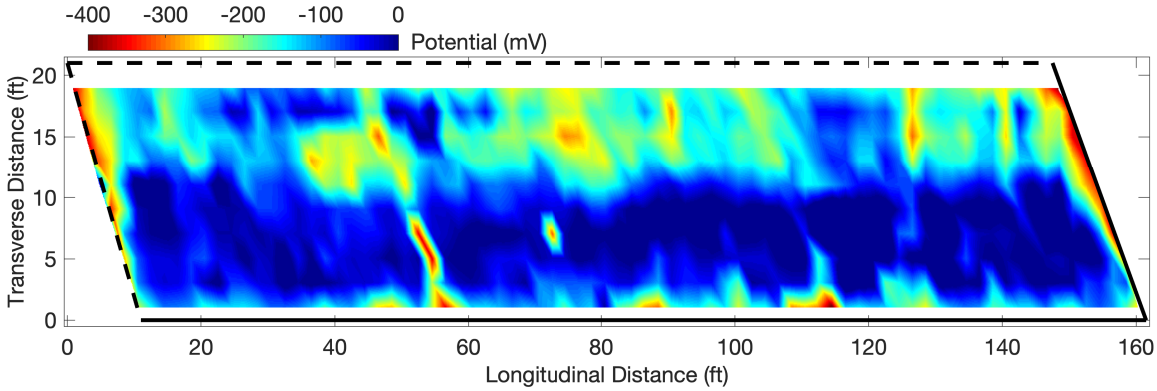

Fig. 3.4. Half-cell potential map of the bridge S075 17596

only on one side of the bridge and the flight had to be paused and resumed multiple times while semi-trailers were passing by. As a result, the stitched image map is warped and missing some important information within the area of interest (Figure 3.5a). In this study, delamination, patched area, and cracks were the type of defects that was inspected with our data analytics tools.

The images collected from the UAV for this bridge had some limitations as discussed above. Traffic control was conducted only on one side of the bridge and data collection was interrupted multiple times. In addition, the image capture from the UAV had to be conducted from a height 16 ft above the bridge deck. This can be improved by having manual control of the UAV for future data collection to improve the resolution of the images being collected. The predictions made from the deep learning model did not show much crack information. In the zoomed image of the top left corner between the expansion joints, some of the transverse cracks were detected from the prediction as shown in Figure 3.5b. These are also the locations in proximity where delamination was identified by NDOT chain drag operation after asphalt removal and later repaired with concrete patches (patches identified in Figure 3.5c).

In the second data collection conducted on the repaired bridge on September 18, most of the images (230 images; 99%) had an overlapping feature which allowed a better stitching result as shown in Figure 3.5c. The stitching results are improved than the image collected on 8/24. Since the images were still collected from 16 ft above the bridge deck, there were not many cracks detected on the bare deck. Yet, the photos do allow to compute the area of patches.

(a) Stitched UAV image collected on asphalt overlaid concrete deck

(b) Closeup view of the left top corner with cracks detected on Bridge S075 17596 (asphalt overlaid concrete deck)

(c) Stitched UAV image of bridge S075 17596 collected on repaired concrete deck

Fig. 3.5. Stitched UAV images of bridge S075 17596 before and after repair

3.2.3 Multi-sensing data analysis of bridge S075 17596

GPR data collected on asphalt overlay and on concrete

GPR data collected on the same bridge on asphalt overlay and bare concrete will allow us to analyze the correlation between two sets of data, and evaluate the effect of asphalt overlay on GPR. GPR amplitude maps on asphalt overlay (Figure 3.3a) and on bare concrete (Figure 3.3b) are in general agreement. For qualitative comparison of these two GPR results, we overlapped the deteriorated areas detected by two GPR scans and showed the overlapped comparison in Figure 3.6.

In Figure 3.6, the red color represents deterioration detected by GPR scans on bare concrete, and the blue color indicates deterioration detected by GPR scans on asphalt overlay. Purple color indicates deterioration detected by both GPR scans. In general, both maps agree with each other in deterioration regions, especially along the cold joint at 10 ft (transverse direction) and a horizontal line at 5ft. Both maps also detect deterioration at the end joints and in the driving lane between 70 ft and 120 ft. However, the GPR data collected on concrete (red) detected more deteriorated areas in the driving lane along a horizontal line at 15 ft in the transverse direction. These areas might have less severe deterioration (light blue color in Figure 3.3b) which was not clearly shown in GPR data collected on asphalt overlay.

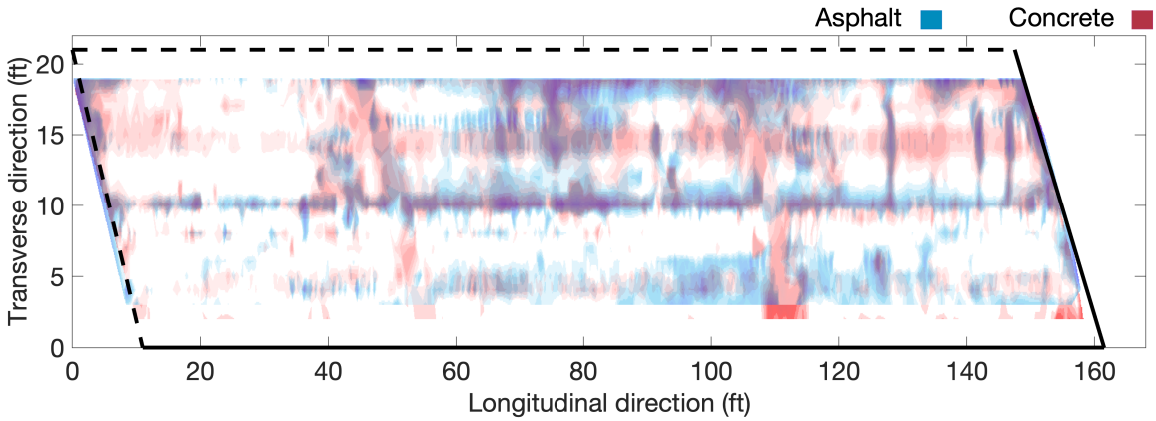

Fig. 3.6. Comparison of GPR maps collected on Bridge S075 17596 on asphalt overlay and on concrete deck

For the purpose of a quantitative comparison, Figure 3.7a shows a scatter plot of GPR rebar amplitudes collected on the same positions on the asphalt and bare concrete. There are 4106 data points in the scatter plot. GPR data on concrete has a slightly larger amplitude

range (-15 dB ~ 6 dB) than the data on asphalt surface (-12 dB ~ 2 dB). It might be caused by different surface reflection amplitudes used in the amplitude normalization procedure [16]. Since the surface reflection amplitude on concrete is smaller than that on the asphalt surface, the normalized GPR amplitudes collected on concrete surface show a larger data range and more scattering. Although a strong relationship is observed in Figure 3.7a, no further conclusion can be drawn regarding the type of relationship between rebar amplitudes in these two data sets. Therefore, an autoencoder was designed and trained as a regression model to determine a relationship between GPR data collected on asphalt and on concrete. Figure 3.7b shows the result of autoencoder output, which gives a nearly linear correlation between GPR amplitudes collected on asphalt and concrete surfaces. The scattered data points were removed by the model, and the GPR data on concrete deck has a smaller data range than before. Since the slope of output line is less than 1.0, it indicates higher rate of attenuation in asphalt overlaid deck than in bare concrete deck for this bridge.

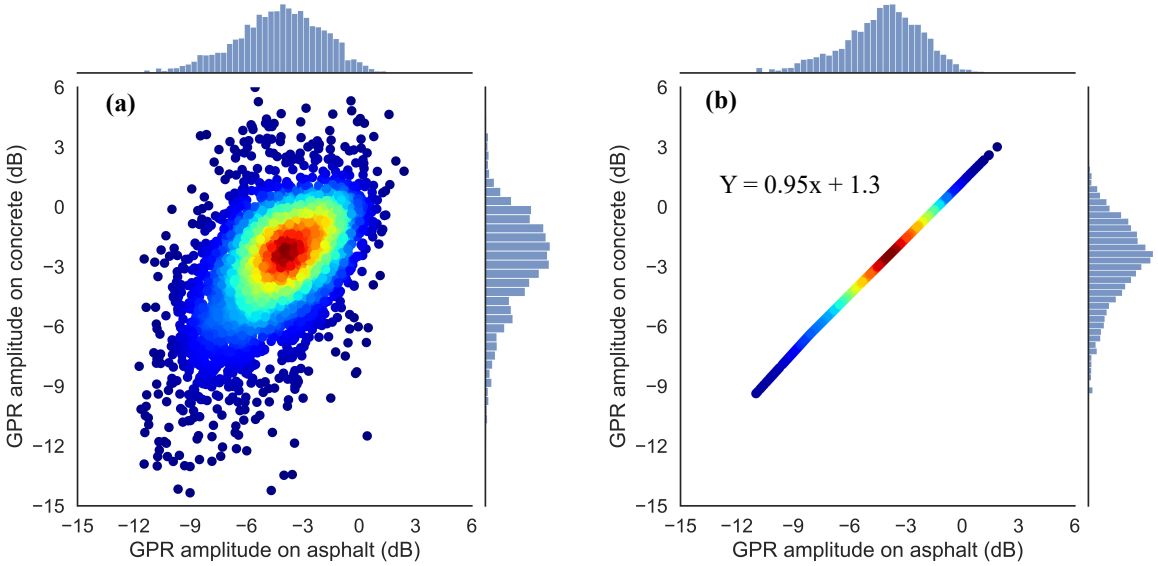

Fig. 3.7. Autoencoder (a) input and (b) output for GPR data collected on asphalt overlay and bare concrete deck

Correlation between GPR and HCP collected on concrete deck

According to ASTM C876 [18], HCP data potential values below -350 mV and above -200 mV are associated with more than 90% and less than 10% probabilities of reinforcement corrosion in concrete. Any voltage measurements between -350 mV and -200 mV in HCP

data are defined as uncertain. By understanding the relationship between GPR and HCP on bare concrete, we can determine the threshold of GPR amplitudes for identification of deterioration in bridge deck. Therefore another autoencoder was designed to determine the relationship between GPR and HCP data collected on the concrete bridge deck.

Figure 3.8a shows the scatter plot of HCP data and average of GPR amplitudes within 1.3 ft radius from HCP grid points. There are 744 data points in this figure. Figure 3.8b shows the output of autoencoder, which gives a strong linear relationship between GPR amplitude and HCP. Based on the linear fitting formula, the voltages of -350 mV and -200 mV correspond to GPR amplitudes (rebar reflection, depth corrected and surface normalized) of -6.4 dB and -4.15 dB, respectively. These two thresholds are used to define color ranges in GPR amplitude maps in Figure 3.3. It should be noted that, since there are not sufficient data points below -350 mV HCP in Figure 3.8a, this relationship might be only accurate for data range above -350 mV, i.e., concrete deck with less severe deterioration.

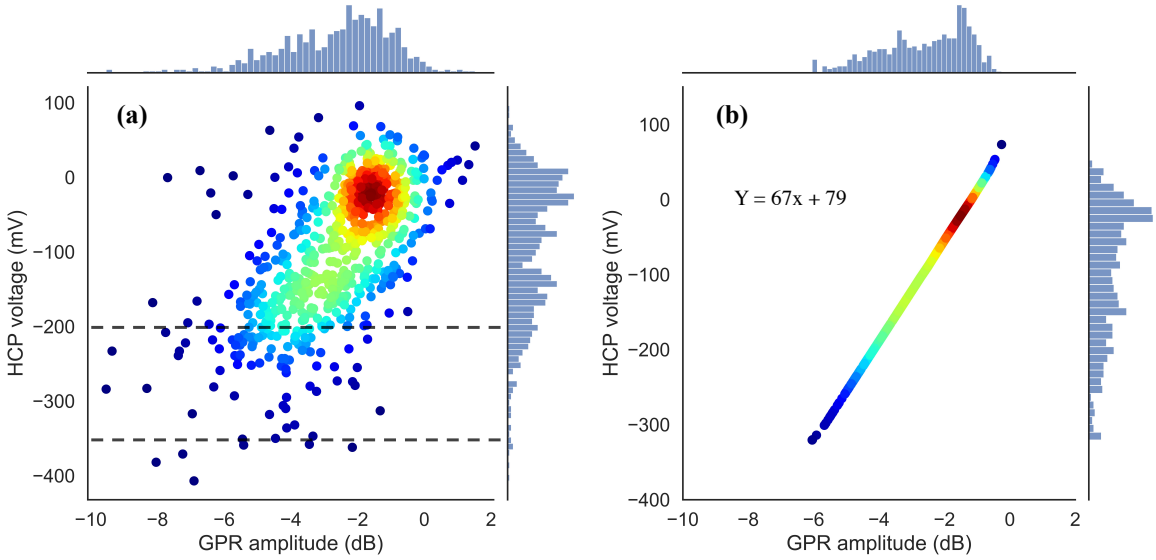

Fig. 3.8. Autoencoder (a) input and (b) output for GPR and HCP data collected on bare concrete

The third autoencoder is designed to determine the relationship between GPR rebar amplitudes collected on asphalt overlay and HCP voltages collected on the bare concrete. Figure 3.9a gives the scatter plot. Unlike in Figure 3.8a, data points in this plot show large scattering. The correlation between GPR on asphalt and HCP is weak and any conclusion from this relationship may not be reliable. Therefore, instead of using the relationship in Figures 3.9b, GPR threshold amplitudes were determined indirectly based on relationship

between GPR and HCP data collected on concrete, and between GPR amplitudes collected on asphalt and on concrete. According to formulas presented in Figures 3.7 b and 3.8, thresholds of -8.1 dB and -5.75 dB was obtained for GPR amplitudes on asphalt with respect to -350 mV and -200 mV in HCP data.

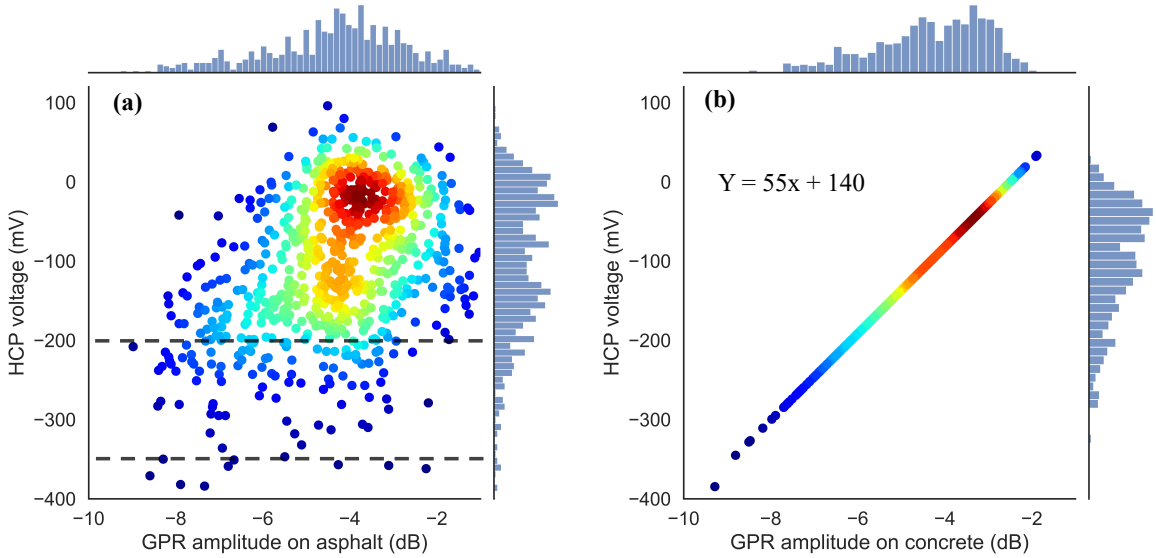

Fig. 3.9. Autoencoder (a) input and (b) output for GPR and HCP data collected on asphalt and bare concrete

Comparison between GPR map and UAV images

Figure 3.10 shows the location of surface defects on asphalt surface that are extracted from the UAV stitched image in Figure 3.5a and then overlapped on the GPR amplitude map collected on the asphalt overlay. Most defects on asphalt overlay correspond to low amplitude on the GPR map, and especially good agreement is obtained along the shoulder joint and the lane divider. Some surface defects near the top right corner are not shown in GPR map on asphalt overlay. Combining information from both GPR and UAV images will provide more accurate evaluation of bridge deck.

In Figure 3.11, locations of repair patches, based on delamination detected by chain-drag, are overlapped with the GPR amplitude map. The visual comparison indicates that most delamination were detected by GPR on asphalt. Since GPR is sensitive to early-stage deterioration, it shows more low amplitude areas than chain-drag. Further studies are needed to determine if GPR data should be used with chain-drag test on concrete deck to guide repairs.

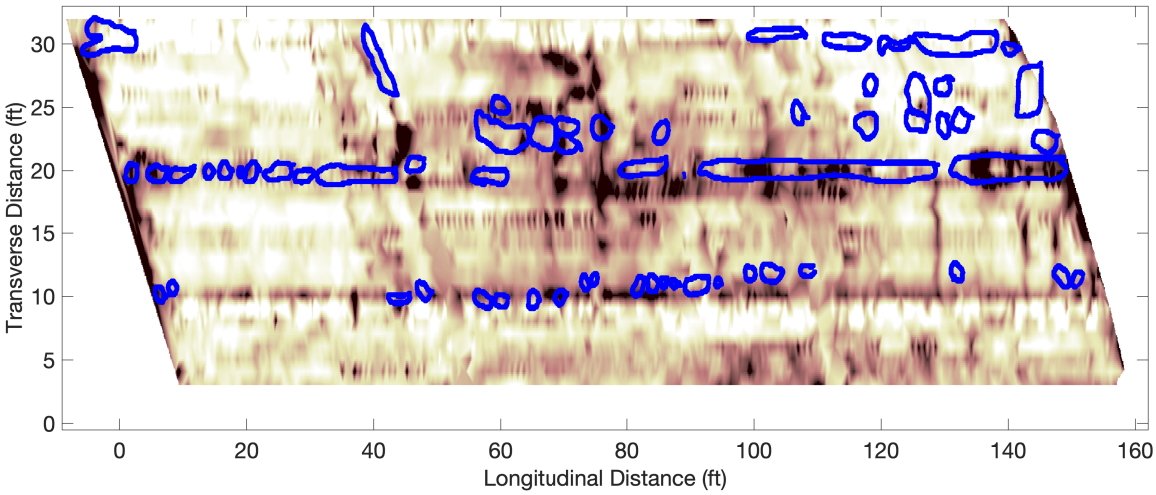

Fig. 3.10. Asphalt surface defects overlapped on GPR amplitude map collected on asphalt overlay

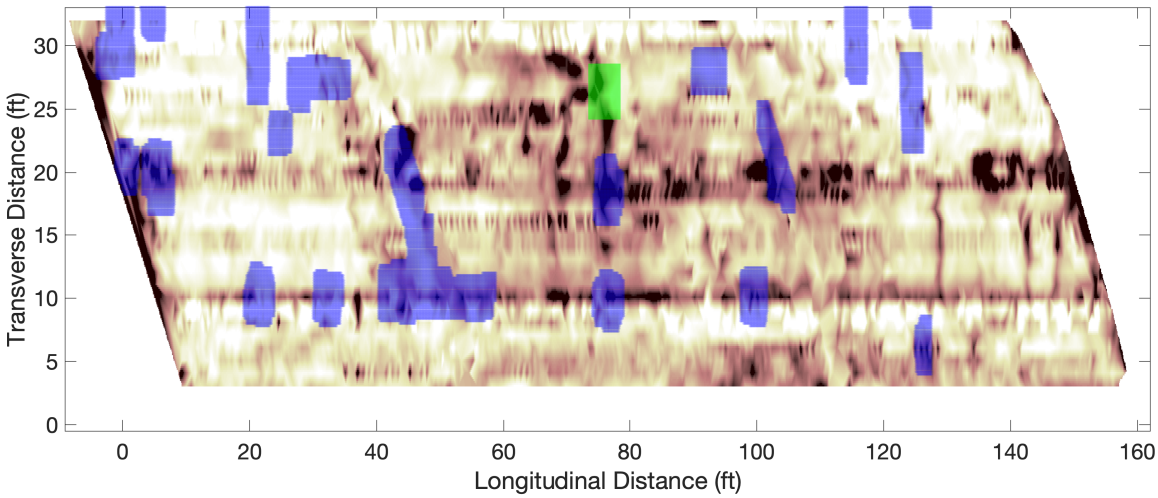

Fig. 3.11. Concrete patches overlapped on GPR amplitude map collected on asphalt overlay

3.3 Bridge 2: S075 17062

3.3.1 Bridge information

Bridge S075 17596 is located on IRR/US75/US77 over the Omaha Creek Tributary in Nebraska, United States. Figure 3.12 shows the satellite image of the bridge. The bridge with three-span deck system is 60 ft long in total and 44 ft in width that carries two-way traffic. This bridge originally had only two driving lanes. In 1974 the bridge was reconstructed, and two shoulders were added to existing lanes. After widening, the bridge received asphalt overlay on a waterproofing membrane. In 2010, a paving project partially removed and replaced the ACC&M overlay. Some deck concrete was repaired with asphalt patches then covered with ACC&M. This work was not completed to meet the current or previous standards. In Figure 3.12, the red solid lines highlight the boundaries of GPR scan region on August 24. The blue dashed lines indicate the boundaries of GPR scan region on August 27 and September 18. For all GPR tests, the resolution of scans was set 3 mm in longitudinal direction and line spacing of 1 ft in lateral direction.

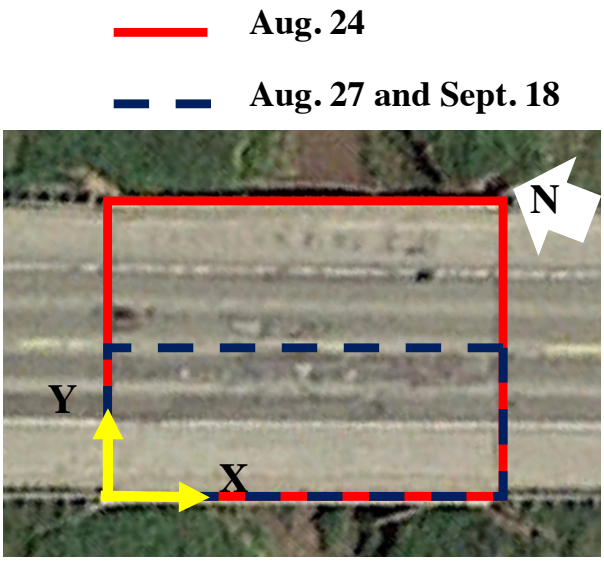

Fig. 3.12. Satellite image of bridge S075 17062

3.3.2 NDT results

Ground Penetrating Radar

GPR data collected on the bridge shows that no top rebar mat was in place for this bridge deck due to large width per length ratio. Consequently, no GPR amplitude map can be generated for this bridge deck. Figure 3.13 shows a B-scan collected on the bridge deck showing that only a few top rebars at the joints of each span. The 1.5 GHz GPR antenna cannot receive reflections from the bottom level rebars. Therefore, GPR data will not be used for data analysis of this bridge deck.

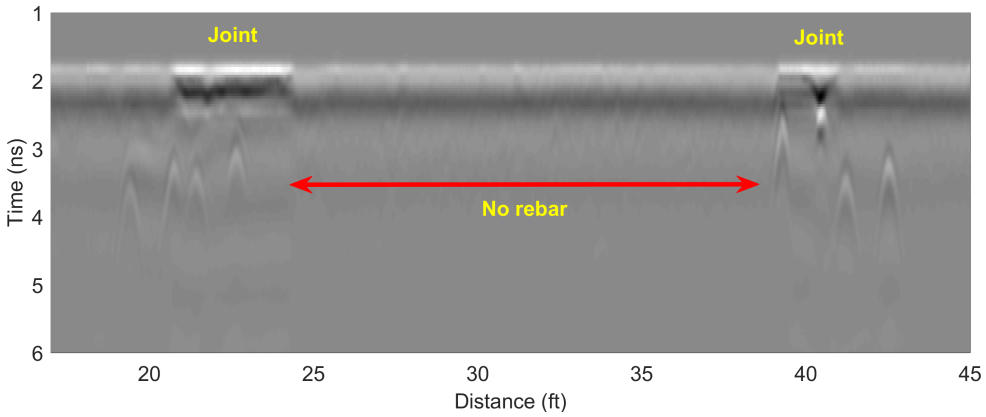

Fig. 3.13. GPR B-scan from the bridge S075 17062 (Google map)

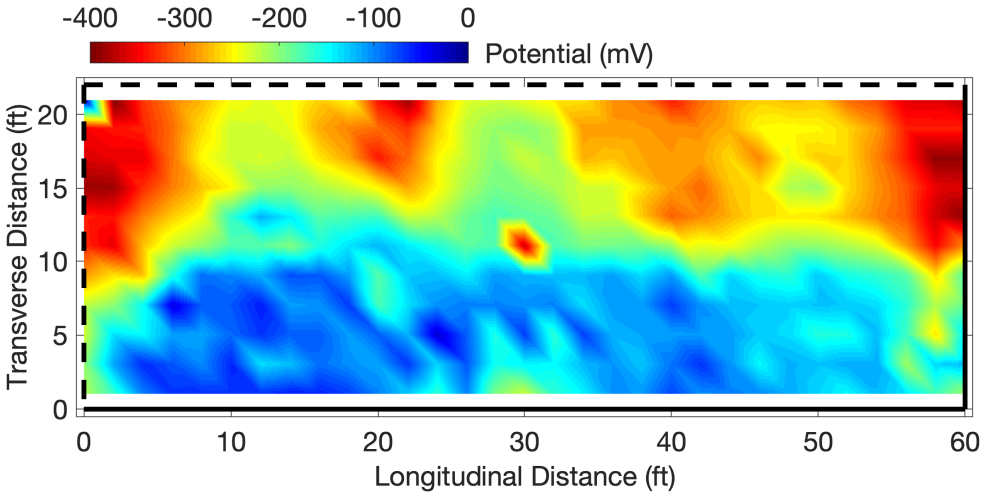

Fig. 3.14. Half cell potential map of the bridge S075 17062

Half-Cell Potential

HCP data was collected on a 2 by 2 ft grid on the bridge deck. To make the electrical circuit, a hole was drilled through the concrete to the bottom rebar level. Figure 3.14 shows the potential map of the bridge deck collected on the western lane and the shoulder as indicated by the blue dashed lines in Figure 3.12. In contrast to shoulder, the driving lane may have high probability of corrosion activity according to the HCP data.

Unmanned Aerial Vehicle Imaging Analysis

A total number of 200 images were collected on August 24 from the Bridge S075 17062 for a 13-minute data collection time and 126 images were collected on September 18 from the identical bridge for a 16-minute data collection time after the deck was repaired. Approximately 6,100 square feet of area was covered from each data collection. In the first data collection conducted on the asphalt overlay bridge on August 24, 98% of the images had sufficient features to allow stitching for the calibrated images. The results are demonstrated on a stitched image map shown in Figure 3.15. Figure 3.15 also shows the crack detection conducted by the deep learning model. It is clearly shown that several transverse cracks are identified within the traffic lane and shoulder of the bridge. The cracks are formed between and in proximity to where the expansion joints are located in this bridge.

Fig. 3.15. Stitched image of asphalt overlaid concrete deck for bridge S075 17062

With the second data collection conducted on the repaired bridge on September 18,

99% of the images collected had an overlapping feature which allowed creating a stitch map as shown in Figure 3.16. The stitched image clearly shows the expansion joints and concrete repair patches. Most patches are along these joints between different spans. The deep learning model predictions identified in Figure 3.16 detects the edges of these patches which helped calculate the area of repair patches. This calculation can help quantify the amount of repair conducted for these bridges with UAV images.

Fig. 3.16. Stitched image for Bridge S075 17062 collected on repaired concrete deck

3.3.3 Multi-sensing data analysis for bridge S075 17062

Figure 3.17 shows location of defects on asphalt overlay overlapped on the HCP map of the bridge deck. Most spalls and old asphalt patches are on the driving lane where the HCP data had more negative voltages. This comparison means surface defects on asphalt overlay may indicate concrete deck deterioration to some degrees, but the surface defect area is much less than the actual deterioration area detected by the HCP measurements.

Figure 3.18 shows the location of new concrete repair patches overlapped on the HCP map. Concrete repair regions were determined based on chain-drag test. The concrete patches agree with the areas with large negative HCP values. However, HCP indicates severe corrosion deterioration at the right joint that was not repaired.

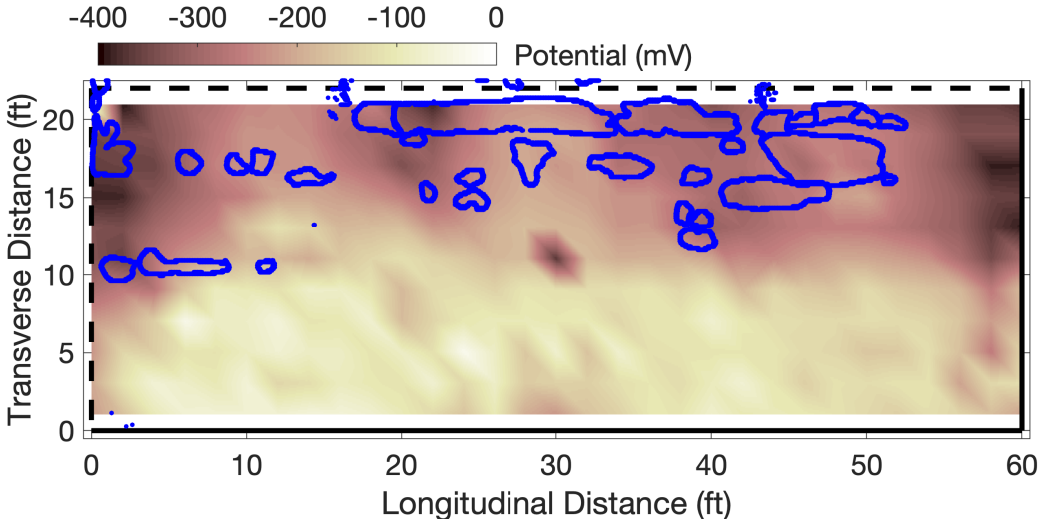

Fig. 3.17. Surface defect locations overlapped on HCP map

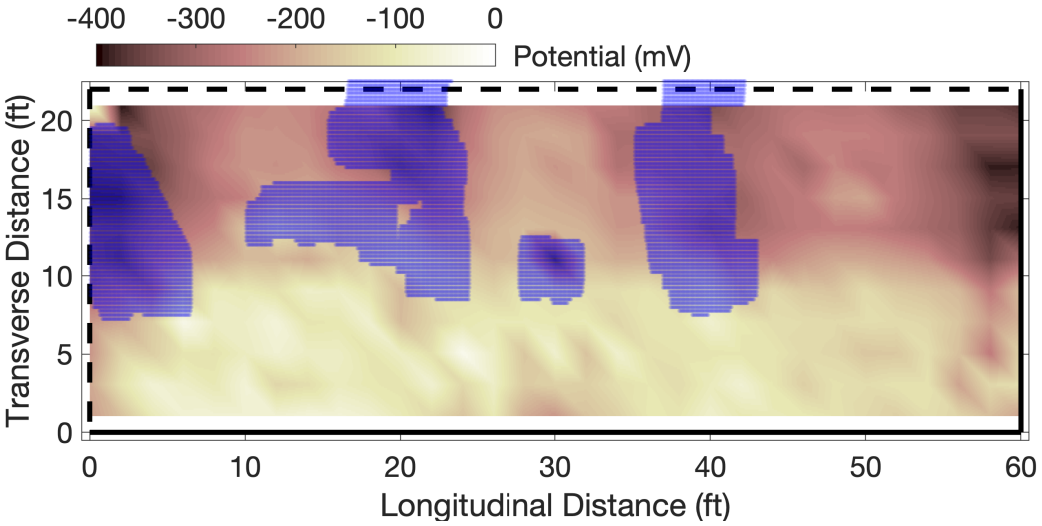

Fig. 3.18. New concrete patch locations overlapped on HCP map

Chapter 4

Conclusions and Future Work

In this research project, two asphalt overlaid bridges were selected by NDOT for demonstration of GPR and UAV imaging system. These NDT techniques (GPR, UAV imaging, and half-cell potential) were performed on the bridge decks during three stages of repair to determine the effectiveness of combining GPR and UAV imaging in evaluation of concrete bridge decks with asphalt overlay.

4.1 Conclusions from GPR and HCP Test Results

GPR scans were conducted on the bridge decks with an old asphalt overlay and on bare concrete decks after asphalt removal. Their results were also compared to the HCP data for quantitative analysis.

GPR threshold analysis

Data analysis shows strong linear relationships between GPR data and HCP data collected on bare concrete, and GPR threshold values can be determined based on the well-established HCP criteria. Comparison between GPR data collected on asphalt overlay and bare concrete deck indicates that GPR can be used on asphalt overlaid bridge decks to detect severe deterioration regions and provide reliable guidance for deck maintenance decision.

Three autoencoders were designed and trained on the GPR and HCP data to model relationships between them. An autoencoder can eliminate noise from the data and obtain a clear relationship between two sets of data. Based on the autoencoder results, two sets of threshold amplitudes were determined for the GPR amplitudes of rebar reflections: (1) on the asphalt overlay, the GPR amplitude of -8.1 dB and -5.75 dB corresponds to -350

Table 4.1. GPR threshold amplitudes based on HCP data

	Probability of Corrosion based on HCP		
Threshold	More than 90%	Uncertain	Less than 10%
GPR on asphalt (dB)	< -8.1	[-8.1, -5.75]	> -5.75
GPR on concrete (dB)	< -6.4	[-6.4, -4.15]	> -4.15
HCP on concrete (mV)	< -350	[-350, -200]	> -200

mV and -200 mV potential in the HCP data, respectively; (2) on the bare concrete, the GPR amplitude of -6.4 dB and -4.15 dB corresponds to -350 mV and -200 mV potential in the HCP data. Based on these values, we may choose proper thresholds and color scales in the GPR amplitude maps to accurately present deteriorated areas. The GPR threshold corresponding to -200 mv HCP value may indicate incipient deterioration of brige deck.

Table 4.1 shows the GPR threshold amplitudes obtained in this research project. Based on autoencoder analysis between the GPR and HCP data collected on bare concrete deck, the GPR amplitude (rebar reflection) threshold is about -6.4 dB, which corresponds to -350 mV in HCP and indicates high possibility of corrosion activities on steel reinforcement. This threshold is close to the value obtained from previous findings by the authors in the M075 project [1, 22]. However, there are not enough data points below the -350 mV HCP threshold in this project. More data should be collected at severe deterioration regions (HCP < -350 mV) to confirm this threshold value.

GPR effectiveness on asphalt overlay

By comparing the detected deterioration areas from the GPR data collected on the asphalt overlay and bare concrete (Figure 3.6), we found that both GPR scans detected the most severe deterioration regions. Purple color on Figure 3.6 indicates agreement in detected deterioration from two GPR maps (with and without asphalt overlay). The GPR data collected on asphalt may missed some mild deterioration area. When proper threshold values are used (e.g. autoencoder analysis from GPR and HCP data), the GPR condition maps collected on asphalt or concrete surface may provide reliable information about deterioration areas and guide bridge deck maintenance decision.

Correlation coefficient can be used to evaluate the level of agreement between two datasets with linear relationship. Correlation coefficient varies between -1 and 1. Values closer to 0 show less linear relationship. Values close to -1 and 1 are indicative of strong negative and positive linear relationships, respectively. Quantitative analysis shows that the

Table 4.2. Correlation coefficient between pairs of NDT data

NDT methods	Correlation coefficient
GPR on asphalt - GPR on concrete (Figure 3.7)	0.52
GPR on concrete - HCP on concrete (Figure 3.8)	0.63
GPR on asphalt - HCP on concrete (Figure 3.9)	0.42

correlation between GPR on the asphalt overlay and GPR on the bare concrete deck has a coefficient of 0.52. For the investigated bridge deck, the GPR amplitude on asphalt shows a slightly higher attenuation than the data on bare concrete. The correlation coefficient between GPR and HCP data collected on bare concrete is 0.63, which indicates a clear correlation between two quantities. GPR data collected on asphalt overlay and HCP potential shows the least linear relationship with the correlation coefficient of 0.42, which is less than the GPR-HCP correlation for data collected on bare concrete. Table 4.2 summarizes the correlation coefficients between different pairs of datasets.

4.2 Conclusions from UAV Imaging Results

In this study, the collected images and important features were compared to the GPR and HCP results to evaluate the effectiveness of UAV imaging in assessment of bridge decks with asphalt overlay and waterproofing membrane. UAV mounted imaging system was used as a systematic visual inspection for bridges. UAV imaging system can capture many localized images from bridge deck surface. Images were later stitched together to produce a high-resolution image map of the entire bridge deck that contains detailed information about location of surface defects (cracks, spalls, potholes) and other anomalies on the surface. UAV imaging system can be implemented by the NDOT maintenance team to fly and collect data before and after repair of bridge decks. More studies are needed to determine whether UAV imaging system is an effective predictor of deck repair locations or quantities. After deck repairs are complete, the area of patches can easily be detected and calculated so that the DOT engineers can quantify the amount of repair and keep track of the data.

UAV imaging system application

In this study, location of patches were identified with the developed deep learning model. A UAV image-based big data pipeline has been constructed so that it can be implemented to multiple bridges. If images can be collected under a controlled data collection scheme

with full traffic control during inspection, the data quality should improve. For crack detection, better quality of images can be obtained when UAVs collect images at a lower height under full traffic control condition. The UAV system can effectively approach inaccessible locations, such as underneath the bridge deck or bridge piers. Based on the team's experience in M075 project, machine vision cameras mounted on a vehicle provided high quality images. The vehicle mounted system can run at a reasonable speed (up to 30 m/h), which is suitable for fast data collection without traffic control.

UAV imaging system results

Comparing to the GPR and HCP data, we found deterioration is occurring at the proximity of surface defects including potholes, spallings, and old asphalt patches identified by the UAV imaging system. However, the total area of surface defects is less than the deterioration area detected by GPR and HCP. Further quantitative analysis is needed to establish the relationship between surface defects and severity of deterioration, which may enable us to use UAV images as an initial screening decision criterion for deploying and extending NDT inspection of bridge decks.

4.3 Implementation Plan and Future Work

In this research project, the UNL team conducted multiple NDT inspections on two Nebraska bridges with ACC&M during different stages of construction. The results of NDT data collection in this project indicated effectiveness of GPR on asphalt overlaid bridge decks. GPR threshold amplitudes were obtained based on correltion analysis between GPR and HCP data. These thresholds might be applied to future GPR evaluation if recommended GPR data processing [16] is followed. These threshold amplitudes help identify the quantity and severity of deteriorated areas based on ASTM D6087 guidelines for HCP. However, more data is needed to build a more reliable correlation between GPR and HCP for severely deteriorated areas.

In M075 project, machine vision cameras mounted on a vehicle provided high quality images. The vehicle mounted imaging system also allows fast data collection without closing traffic. UAV based imaging can be used as a supplementary method to collect images at regions hard to access, or the bottom side of bridge decks.

Ground-coupled GPR data collection is usually performed at the walking speed. Air-coupled GPR is able to scan the bridge deck at the traffic speed. Air-coupled GPR might be

combined with vehicle-mounted imaging system for fast and comprehensive evaluation of bridge decks. Because air-coupled GPR has lower spatial resolution than ground-coupled GPR, further study is needed to collect data with both systems on the same bridges and compare their performance.

The long-term goal is to implement air-coupled GPR and vehicle-mounted imaging system for regular bridge deck inspection. The GPR attenuation map and the surface defects detected from high-resolution images will provide reliable evaluation of bridge decks.

Bibliography

[1] S. Pashoutani, J. Zhu, C. Sim, B. Mazzeo, and S. Guthrie, "Development and implementation of a moving nondestructive evaluation platform for bridge deck inspection," Final Report SPR-P1(17) (M075), 2020.

[2] T. Oh, S.-H. Kee, R. W. Arndt, J. S. Popovics, and J. Zhu, "Comparison of ndt methods for assessment of a concrete bridge deck," *Journal of Engineering Mechanics*, vol. 139, no. 3, pp. 305–314, 2013.

[3] S.-H. Kee, T. Oh, J. S. Popovics, R. W. Arndt, and J. Zhu, "Nondestructive bridge deck testing with air-coupled impact-echo and infrared thermography," *Journal of Bridge Engineering*, vol. 17, no. 6, pp. 928–939, 2012.

[4] ASTM D6087 - 08(2015)E1, "Standard test method for evaluating asphalt-covered concrete bridge decks using ground penetrating RADAR," West Conshohocken, PA: American Society for Testing and Materials, 2015.

[5] K. Dinh, N. Gucunski, J. Kim, and T. H. Duong, "Understanding depth-amplitude effects in assessment of GPR data from concrete bridge decks," *NDT & E International*, vol. 83, pp. 48 – 58, 2016.

[6] A. Tarussov, M. Vandry, and A. De La Haza, "Condition assessment of concrete structures using a new analysis method: Ground-penetrating radar computer-assisted visual interpretation," *Construction and Building Materials*, vol. 38, pp. 1246–1254, Jan. 2013.

[7] "AASHTO Survey Finds Drone Use Exploding Among State DOTs," *AASHTO Journal*, May 2019.

[8] T. Yamaguchi and S. Hashimoto, "Fast crack detection method for large-size con-

crete surface images using percolation-based image processing," *Machine Vision and Applications*, vol. 21, pp. 797–809, 2009.

[9] P. Prasanna, K. J. Dana, N. Gucunski, B. B. Basily, H. M. La, R. S. Lim, and H. Parvardeh, "Automated crack detection on concrete bridges," *IEEE Transactions on Automation Science and Engineering*, vol. 13, no. 2, pp. 591–599, 2016.

[10] C. Yeum and S. J. Dyke, "Vision-based automated crack detection for bridge inspection," *Computer-Aided Civil and Infrastructure Engineering*, vol. 30, pp. 759–770, 2015.

[11] F.-C. Chen and M. R. Jahanshahi, "NB-CNN: Deep learning-based crack detection using convolutional neural network and naive bayes data fusion," *IEEE Transactions on Industrial Electronics*, vol. 65, no. 5, pp. 4392–4400, 2017.

[12] A. Mohan and S. Poobal, "Crack detection using image processing," *Alexandria Engineering Journal*, vol. 57, no. 2, pp. 787–798, 2018.

[13] Z. Liu, Y. Cao, Y. Wang, and W. Wang, "Computer vision-based concrete crack detection," *Automation in Construction*, vol. 104, pp. 129–139, 2019.

[14] M. Alipour and D. K. Harris, "Increasing the robustness of material-specific deep learning models for crack detection across different materials," *Engineering Structures*, vol. 206, no. 110157, 2020.

[15] K. Won and C. Sim, "Automated transverse crack mapping system with optical sensors and big data analytics," *Sensors*, vol. 20, no. 7: 1838, 2020.

[16] S. Pashoutani and J. Zhu, "Ground penetrating radar data processing for concrete bridge deck evaluation," *Journal of Bridge Engineering*, vol. 25, will appear in 2020.

[17] S. Pashoutani and J. Zhu, "Condition assessment of concrete bridge deck with asphalt overlay," Final report Nebraska Department of Transportation SPR-P1(17) M065, 2019.

[18] ASTM C876-15, "Standard test method for corrosion potentials of uncoated reinforcing steel in concrete," West Conshohocken, PA: American Society for Testing and Materials, 2015.

[19] H. Kaiming, G. Gkioxari, P. Dollar, and R. Girshick, "Mask R-CNN," *Proceedings of the IEEE International Conference on Computer Vision (ICCV)*, pp. 2961 – 2969, 2017.

[20] S. Ren, H. Kaiming, R. Girshick, and J. Sun, "Faster R-CNN: Towards real-time object detection with region proposal networks," *Advances in Neural Information Processing Systems*, pp. 91 – 99, 2015.

[21] H. Sun, S. Pashoutani, and J. Zhu, "Nondestructive evaluation of concrete bridge decks with automated acoustic scanning system and Ground Penetrating RADAR," *Sensors*, vol. 18, no. 6, p. 1955, 2018.

[22] S. Pashoutani, J. Zhu, C. Sim, K. Won, B. A. Mazzeo, and W. S. Guthrie, "Multi-sensor data collection and fusion using autoencoders in condition evaluation of concrete bridge decks," *Journal of Infrastructure Preservation and Resilience*, vol. 2, no. 18, 2021.